1

Paper 1

Revisiting the stability analysis of the flow over a rotating disk

By E. Appelquist[1,2] and Shintaro Imayama[1]

[1]Linné FLOW Centre, KTH Mechanics, SE-100 44 Stockholm, Sweden
[2]Swedish e-Science Research Centre (SeRC)

Technical report, 2014

Local linear stability analysis applied to the rotating-disk flow is discussed. This flow case is an exact similarity solution to the cylindrical incompressible Navier–Stokes equations also called the von Kármán flow. The laminar mean velocity profiles are obtained by solving the resulting ordinary differential equations assuming the flow is axisymmetric and time independent. Two stability-analyses methods are used to investigate the local linear stability of this flow: i) the 'shooting method'; and ii) the 'Chebyshev polynomial method'. This theoretical investigation focuses on convectively unstable disturbances. Results obtained from the two methods are compared and the methods are shown to give similar results. These theoretical results are also compared with direct numerical simulations and experimental results showing good agreement.

---

1. Introduction

The rotating-disk flow has been investigated, not only as a simple model of three-dimensional boundary-layer cross-flow instability, but also since this flow has applications to rotating flow configurations such as the turbomachinery, computer storage devices and chemical vapour deposition (CVD). The flow is induced by a disk rotating without any externally imposed flow. The resulting boundary layer is known as the 'von Kármán boundary layer', which belongs to a family of rotating boundary layers, so called 'BEK boundary layers', including Bödewadt, Ekman and von Kármán boundary layers. These boundary layers are characterized by a Rossby number Ro, which is defined as

$$Ro = \frac{\Omega_f^* - \Omega_d^*}{\Omega_a^*} \tag{1}$$

with $\Omega_a^* = (\Omega_f^* + \Omega_d^*)/4 + ((\Omega_f^* + \Omega_d^*)^2/16 + (\Omega_f^* - \Omega_d^*)^2/2)^{1/2}$, where Ω_f^* and Ω_d^* are the fluid angular velocity outside the boundary layer and the disk angular velocity, respectively (Arco *et al.* 2005). For the von Kármán boundary layer $Ro = -1$ since Ω_f^* is 0. The second important parameter for this flow is the

Reynolds number, which is the ratio between inertial forces and viscous forces. This is given as

$$R = r^* \sqrt{\frac{\Omega^*}{\nu}}, \tag{2}$$

where r^* is the radius of the disk at the measurement position, Ω^* is the angular velocity of the disk, ν is the kinematic viscosity of the fluid and * denotes a dimensional quantity. The rotating-disk flow is a three dimensional boundary layer with an inflection point in the radial velocity profile which makes the flow inviscidly unstable according to the Rayleigh stability criterion.

A linear stability analysis has been performed on the rotating-disk flow in earlier studies (e.g. Kobayashi *et al.* 1980; Malik *et al.* 1981; Mack 1985; Malik 1986; Faller 1991; Lingwood 1995*a*; Hussain *et al.* 2011), and it was found that the rotating-disk flow has instabilities consisting of stationary and travelling disturbances, and also has two types of instabilities, namely one due to an inviscid mechanism attributed an inflection point of radial velocity profile and one due to a viscid mechanism including centrifugal and Coriolis forces. The main purpose of this report is to discuss local linear stability analysis and its application to the rotating-disk flow. In this report, the following problems are discussed. First, the laminar mean velocity profile is obtained solving the exact axisymmetric similarity solution of the Navier–Stokes equations for the time independent von Kármán boundary layer. Secondly, local linear stability analysis of the rotating-disk flow is discussed. Local linear stability analysis was developed to evaluate the stability of a flow when assuming small disturbances justifying a linearization of the equations, and assuming a homogeneous flow in the streamwise direction. Two different methods for the local linear stability analysis are introduced: the 'shooting method'; and the 'Chebyshev polynomial method'. Finally, results obtained from the two methods are compared with direct numerical simulations (DNS) and experimental results.

2. Governing equations

The similarity solution governing the mean flow over a rotating disk is presented here together with the perturbation equations which govern the linear local stability of the rotating-disk flow. The description of the flow originates from the Navier–Stokes equations formulated in a cylindrical-coordinate system in the rotating frame of reference. For the perturbation equations, the parallel-flow approximation is used to simplify the partial-differential system of equations (PDE) to a sixth-order system of ordinary-differential equations (ODE). The meaning of this simplification is that only the local stability behaviour will be analysed. There is a possibility to further reduce the set of equations neglecting the Coriolis and streamline-curvature terms leading to the Orr-Sommerfeld equation. By also neglecting viscosity the equations are reduced to the Rayleigh equation. However, in this context only the sixth-order

system of ODE will be considered, including rotation and curvature. The path taken for the derivation of the equations is the same as in Lingwood (1995*b*).

2.1. *Mean flow*

The disk is assumed to be of infinite radius, rotating with a constant angular velocity around an axis passing through the centre of the disk in an incompressible fluid. The equations governing the flow over the rotating disk are the incompressible Navier–Stokes and the continuity equations in cylindrical coordinates (r, θ, z),

$$\frac{\partial U^*}{\partial t^*} + \mathbf{U}^* \cdot \nabla U^* - \frac{V^{*2}}{r^*} - 2\Omega^* V^* - \Omega^{*2} r^* = -\frac{1}{\rho}\frac{\partial P^*}{\partial r^*} + \nu\Big(\nabla^2 U^* - \frac{U^*}{r^{*2}} - \frac{2}{r^{*2}}\frac{\partial V^*}{\partial \theta}\Big), \tag{3}$$

$$\frac{\partial V^*}{\partial t^*} + \mathbf{U}^* \cdot \nabla V^* + \frac{U^* V^*}{r^*} + 2\Omega^* U^* = -\frac{1}{r^*\rho}\frac{\partial P^*}{\partial \theta} + \nu\Big(\nabla^2 V^* + \frac{2}{r^{*2}}\frac{\partial U^*}{\partial \theta} - \frac{V^*}{r^{*2}}\Big), \tag{4}$$

$$\frac{\partial W^*}{\partial t^*} + \mathbf{U}^* \cdot \nabla W^* = -\frac{1}{\rho}\frac{\partial P^*}{\partial z} + \nu\nabla^2 W^*, \tag{5}$$

$$\frac{\partial U^*}{\partial r^*} + \frac{U^*}{r^*} + \frac{1}{r^*}\frac{\partial V^*}{\partial \theta} + \frac{\partial W^*}{\partial z^*} = 0, \tag{6}$$

where U, V and W are the radial, azimuthal and vertical velocities and P is the pressure. ν is the kinematic viscosity, ρ is the density, Ω is the rotation rate and t is time. The star superscript means that the quantities are dimensional. Included are the centrifugal force and the Coriolis force, respectively, $-\Omega^* \mathbf{e_z} \times (\Omega^* \mathbf{e_z} \times r^* \mathbf{e_r}) = \Omega^{*2} r^* \mathbf{e_r}$ and $-2\Omega^* \mathbf{e_z} \times \mathbf{U}^* = 2\Omega^* V^* \mathbf{e_r} - 2\Omega^* U^* \mathbf{e}_\theta$, where $\mathbf{e_r}$, $\mathbf{e}_\theta$ and $\mathbf{e_z}$ are the unit vectors in each direction.

The similarity variables used are functions of z alone. For the global scale these are $U(z) = U^*/(r^*\Omega^*)$, $V(z) = V^*/(r^*\Omega^*)$, $W(z) = W^*/(\nu\Omega^*)^{1/2}$, $P(z) = P^*/(\rho\nu\Omega^*)$, $z = z^*/L^*$ and $r = r^*/L^*$ where $L^* = (\nu/\Omega^*)^{1/2}$. The nondimensional Reynolds number can be rewritten by using the similarity variables

$$R = \frac{r^*\Omega^* L^*}{\nu} = r^* \frac{1}{L^{*2}} L^* = \frac{r^*}{L^*} = r, \tag{7}$$

that is, the Reynolds number equals the nondimensional radius. Using these global scale similarity variables in the governing equations, equations (3)–(6), and assuming that the base flow is independent of θ and steady in time, the

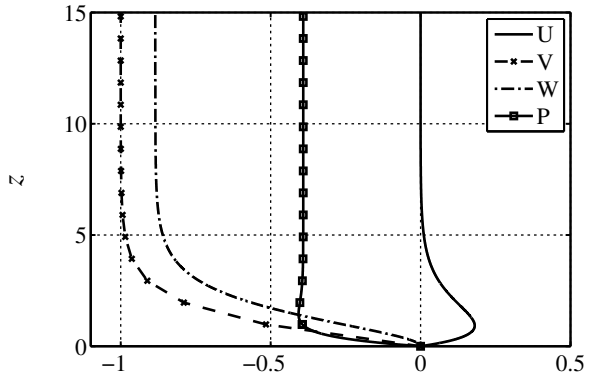

FIGURE 1. The similarity solution for the flow over a rotating disk. The solution is shown in the rotating reference frame where U, V and W are the radial, azimuthal and vertical velocity components, and P is the pressure.

following system of ODEs is obtained

$$2U + W' = 0 \tag{8}$$

$$U^2 - (V+1)^2 + U'W - U'' = 0 \tag{9}$$

$$2U(V+1) + V'W - V'' = 0 \tag{10}$$

$$P' + WW' - W'' = 0 \tag{11}$$

where the prime denotes differentiation with respect to z. These are the equations first derived by von Kármán (1921). Here, the above equations were solved using the Runge–Kutta fourth order (RK4) method with a Newton–Raphson searching method. The resulting velocity and pressure profiles are seen in figure 1. The appendix gives a closer description of the solution method.

2.2. *Perturbation equations*

In deriving the perturbation equations, again equations (3)–(6) are used, however, this time all the terms are kept and made dimensionless with respect to the local scale similarity variables $U(z) = U^*/(r_s^*\Omega^*)$, $V(z) = V^*/(r_s^*\Omega^*)$, $W(z) = W^*/(r_s^*\Omega^*)$, $P(z) = P^*/(\rho r_s^{*2}\Omega^{*2})$, $z = z^*/L^*$, $r = r^*/L^*$ where $L^* = (\nu/\Omega^*)^{1/2}$. The Reynolds number is now written in terms of the local radial position $R = r_s^*\Omega^*L^*/\nu = r_s^*/L^* = r_s$ and also $t = t^*/(L^*/\Omega^* r_s^*)$. The local scale is justified by assuming a parallel-flow, also enforced later on. The difference between the global and the local scale is mainly the use of the local radius r_s^* instead of the global r^*. Also, the W and P terms are scaled differently and a time scale is introduced. Using the above nondimensional variables

in equations (3)–(6) gives the dimensionless governing equations for the local scale. Then decomposing these into a mean and a perturbation quantity by the use of

$$U(z,r,\theta,t) = \frac{r}{R}U(z) + u(z,r,\theta,t) \tag{12}$$

$$V(z,r,\theta,t) = \frac{r}{R}V(z) + v(z,r,\theta,t) \tag{13}$$

$$W(z,r,\theta,t) = \frac{1}{R}W(z) + w(z,r,\theta,t) \tag{14}$$

$$P(z,r,\theta,t) = \frac{1}{R^2}P(z) + p(z,r,\theta,t) \tag{15}$$

and subtracting the first given dimensionless governing equations, yields the nonlinear perturbation equations. Linearizing with respect to the perturbation quantities leads to the perturbation equations for continuity

$$\frac{\partial u}{\partial r} + \frac{u}{r} + \frac{1}{r}\frac{\partial v}{\partial \theta} + \frac{\partial w}{\partial z} = 0 \tag{16}$$

and momentum conservation in the radial direction

$$\begin{aligned}\frac{\partial u}{\partial t} + \frac{rU}{R}\frac{\partial u}{\partial r} + \frac{uU}{R} + \frac{V}{R}\frac{\partial u}{\partial \theta} + \frac{W}{R}\frac{\partial u}{\partial z} + \frac{rwU'}{R} - \frac{2Vv}{R} - \frac{2v}{R} \\ = -\frac{\partial p}{\partial r} + \frac{1}{R}\left(\frac{\partial^2 u}{\partial r^2} + \frac{1}{r^2}\frac{\partial^2 u}{\partial \theta^2} + \frac{\partial^2 u}{\partial z^2} + \frac{1}{r}\frac{\partial u}{\partial r} - \frac{u}{r^2} - \frac{2}{r^2}\frac{\partial v}{\partial \theta}\right),\end{aligned} \tag{17}$$

in the θ direction

$$\begin{aligned}\frac{\partial v}{\partial t} + \frac{rU}{R}\frac{\partial v}{\partial r} + \frac{V}{R}\frac{\partial v}{\partial \theta} + \frac{W}{R}\frac{\partial v}{\partial z} + \frac{rwV'}{R} + \frac{Uv}{R} + \frac{2uV}{R} + \frac{2u}{R} \\ = -\frac{1}{r}\frac{\partial p}{\partial \theta} + \frac{1}{R}\left(\frac{\partial^2 v}{\partial r^2} + \frac{1}{r^2}\frac{\partial^2 v}{\partial \theta^2} + \frac{\partial^2 v}{\partial z^2} + \frac{1}{r}\frac{\partial v}{\partial r} - \frac{v}{r^2} + \frac{2}{r^2}\frac{\partial u}{\partial \theta}\right)\end{aligned} \tag{18}$$

and in the z-direction

$$\begin{aligned}\frac{\partial w}{\partial t} + \frac{rU}{R}\frac{\partial w}{\partial r} + \frac{V}{R}\frac{\partial w}{\partial \theta} + \frac{W}{R}\frac{\partial w}{\partial z} + \frac{wW'}{R} \\ = -\frac{\partial p}{\partial z} + \frac{1}{R}\left(\frac{\partial^2 w}{\partial r^2} + \frac{1}{r^2}\frac{\partial^2 w}{\partial \theta^2} + \frac{\partial^2 w}{\partial z^2} + \frac{1}{r}\frac{\partial w}{\partial r}\right).\end{aligned} \tag{19}$$

Here, to make the equations separable in r, θ and t the parallel-flow approximation is made, meaning that the variation of Reynolds number with radius can be ignored, thus replacing the radius r with R, the local Reynolds number. Then neglecting terms in the order of $1/R^2$ the perturbation equations become, in the same sequence as above,

$$\frac{\partial u}{\partial r} + \frac{u}{R} + \frac{1}{R}\frac{\partial v}{\partial \theta} + \frac{\partial w}{\partial z} = 0 \tag{20}$$

$$\frac{\partial u}{\partial t}+U\frac{\partial u}{\partial r}+\frac{uU}{R}+\frac{V}{R}\frac{\partial u}{\partial\theta}+\frac{W}{R}\frac{\partial u}{\partial z}+wU'-\frac{2Vv}{R}-\frac{2v}{R} = -\frac{\partial p}{\partial r}+\frac{1}{R}\left(\frac{\partial^2 u}{\partial r^2}+\frac{1}{R^2}\frac{\partial^2 u}{\partial\theta^2}+\frac{\partial^2 u}{\partial z^2}\right) \tag{21}$$

$$\frac{\partial v}{\partial t}+U\frac{\partial v}{\partial r}+\frac{V}{R}\frac{\partial v}{\partial\theta}+\frac{W}{R}\frac{\partial v}{\partial z}+wV'+\frac{Uv}{R}+\frac{2uV}{R}+\frac{2u}{R} = -\frac{1}{R}\frac{\partial p}{\partial\theta}+\frac{1}{R}\left(\frac{\partial^2 v}{\partial r^2}+\frac{1}{R^2}\frac{\partial^2 v}{\partial\theta^2}+\frac{\partial^2 v}{\partial z^2}\right) \tag{22}$$

$$\frac{\partial w}{\partial t}+U\frac{\partial w}{\partial r}+\frac{V}{R}\frac{\partial w}{\partial\theta}+\frac{W}{R}\frac{\partial w}{\partial z}+\frac{wW'}{R} = -\frac{\partial p}{\partial z}+\frac{1}{R}\left(\frac{\partial^2 w}{\partial r^2}+\frac{1}{R^2}\frac{\partial^2 w}{\partial\theta^2}+\frac{\partial^2 w}{\partial z^2}\right). \tag{23}$$

Note that the term including the second derivative in the azimuthal direction was not removed. This is due to the introduction of the global azimuthal wavenumber β later, reducing it to local scale, $\beta=\bar{\beta}R$ eliminating R^2 in the denominator making these terms comparable in size to the other terms. The above perturbation equations can be expressed in normal-mode form

$$u = \hat{u}(z,\alpha,\omega;\beta,R)e^{i(\alpha r+\beta\theta-\omega t)} \tag{24}$$

$$v = \hat{v}(z,\alpha,\omega;\beta,R)e^{i(\alpha r+\beta\theta-\omega t)} \tag{25}$$

$$w = \hat{w}(z,\alpha,\omega;\beta,R)e^{i(\alpha r+\beta\theta-\omega t)} \tag{26}$$

$$p = \hat{p}(z,\alpha,\omega;\beta,R)e^{i(\alpha r+\beta\theta-\omega t)} \tag{27}$$

where the eigenvalue problem is solved for either α or ω. Here, the hat quantities are the spectral representations of the perturbation fields, ω is the frequency of the disturbance and α and β are the radial and azimuthal wavenumbers, respectively. Substituting equations (24)–(27) into equations (20)–(23), the perturbation equations become

$$\left(i\alpha+\frac{1}{R}\right)\hat{u}+\left(\frac{i\beta}{R}\right)\hat{v}+\hat{w}'=0, \tag{28}$$

$$\left(i\alpha U+\frac{i\beta V}{R}+\frac{\alpha^2}{R}+\frac{\beta^2}{R^3}+\frac{U}{R}\right)\hat{u}+\frac{W}{R}\hat{u}'-\frac{1}{R}\hat{u}''-\frac{2}{R}(1+V)\hat{v}+U'\hat{w}+i\alpha\hat{p}=i\hat{u}\omega, \tag{29}$$

$$\frac{2}{R}(V+1)\hat{u}+\left(i\alpha U+\frac{i\beta V}{R}+\frac{\alpha^2}{R}+\frac{\beta^2}{R^3}+\frac{U}{R}\right)\hat{v}+\frac{W}{R}\hat{v}'-\frac{1}{R}\hat{v}''+V'\hat{w}+\frac{i\beta}{R}\hat{p}=i\hat{v}\omega, \tag{30}$$

$$\left(i\alpha U+\frac{i\beta V}{R}+\frac{\alpha^2}{R}+\frac{\beta^2}{R^3}+\frac{W'}{R}\right)\hat{w}+\frac{W}{R}\hat{w}'-\frac{1}{R}\hat{w}''+\hat{p}'=i\hat{w}\omega. \tag{31}$$

Various works, have been done when it comes to the stability analysis of the perturbation equations, either using primitive variables (Balakumar & Malik 1990) or transformed variables (Mack 1985; Malik 1986; Faller 1991; Lingwood 1995*b*; Hwang & Lee 2000). For the two methods used within this paper,

the Chebyshev polynomial method uses primitive variables and the shooting method follows the work of Lingwood (1995*b*) and thus the transformed variables

$$\phi_1(z,\alpha,\omega;\beta,R) = (\alpha - i/R)\hat{u} + \bar{\beta}\hat{v} \tag{32}$$
$$\phi_2(z,\alpha,\omega;\beta,R) = (\alpha - i/R)\hat{u}' + \bar{\beta}\hat{v}' \tag{33}$$
$$\phi_3(z,\alpha,\omega;\beta,R) = \hat{w} \tag{34}$$
$$\phi_4(z,\alpha,\omega;\beta,R) = \hat{p} \tag{35}$$
$$\phi_5(z,\alpha,\omega;\beta,R) = (\alpha - i/R)\hat{v} - \bar{\beta}\hat{u} \tag{36}$$
$$\phi_6(z,\alpha,\omega;\beta,R) = (\alpha - i/R)\hat{v}' - \bar{\beta}\hat{u}' \tag{37}$$

are used giving the equations

$$\phi_1' = \phi_2 \tag{38}$$

$$\frac{\phi_2'}{R} = \frac{1}{R}(X+U)\phi_1 + \frac{W\phi_2}{R} + \left(\left(\alpha - \frac{i}{R}\right)U' + \bar{\beta}V'\right)\phi_3 + i\left(\alpha^2 + \bar{\beta}^2 - \frac{\alpha i}{R}\right)\phi_4 - \frac{2(1+V)\phi_5}{R} \tag{39}$$

$$\phi_3' = -i\phi_1 \tag{40}$$

$$\phi_4' = \frac{iW\phi_1}{R} - \frac{i\phi_2}{R} - \frac{1}{R}(X+W')\phi_3 \tag{41}$$

$$\phi_5' = \phi_6 \tag{42}$$

$$\frac{\phi_6'}{R} = \frac{2(1+V)\phi_1}{R} + \left(\left(\alpha - \frac{i}{R}\right)V' - \bar{\beta}U'\right)\phi_3 + \frac{\bar{\beta}\phi_4}{R} + \frac{1}{R}(X+U)\phi_5 + \frac{W\phi_6}{R} \tag{43}$$

where $X = \alpha^2 + \bar{\beta}^2 + iR(\alpha U + \bar{\beta}V - \omega)$ and $\bar{\beta} = \beta/R$. These transformed equations are assumed to govern the flow from now on, thus including the viscous, Coriolis and streamline-curvature effects.

3. Solution Methods

In this section, two methods for solving the perturbation equations are discussed. The first method is the shooting method, inherited from the work of Lingwood (1995*b*) and used to solve equations (5)–(43). The second method is the Chebyshev polynomial method. This method solves the eigenvalue problems of the perturbation equations (28)–(31) using Chebyshev discretization of the wall-normal coordinate.

3.1. *Shooting method*

The shooting method considers one R with a set of α, β and ω in every iteration, evaluating if these are eigenvalues of the system. The method starts by considering the asymptotic versions of equations (5)–(43) for $z \to \infty$. By doing so, exact closed-form solutions can be obtained at the top boundary and an integration procedure using RK4 method can be used to obtain the solutions

for z positions down to zero. If the solutions match the boundary conditions at $z = 0$ the eigenvalues and eigenfunctions are found. If not, and the values of α, β and ω are estimated well enough, it is possible to tune the chosen shooting variable via a Newton–Raphson searching method and shoot again in order to match the boundary conditions this time and thus find the eigenvalues. The procedure is described in detail in this section and consists of three main steps; (i) calculating the initial values at the top of the domain; (ii) solving the equations by RK4 when stepping down to $z = 0$ and; (iii) evaluating the solution at $z = 0$ in terms of how well it satisfies the boundary conditions.

When $z \to \infty$ equations (5)–(43) take the form

$$\begin{aligned}
\phi_1' &= \phi_2 && (44)\\
\phi_2' &= Y\phi_1 + W_\infty\phi_2 + iR(\alpha^2 + \bar{\beta}^2 - \alpha i/R)\phi_4 && (45)\\
\phi_3' &= -i\phi_1 && (46)\\
\phi_4' &= (iW_\infty\phi_1 - i\phi_2 - Y\phi_3)/R && (47)\\
\phi_5' &= \phi_6 && (48)\\
\phi_6' &= \bar{\beta}\phi_4 + Y\phi_5 + W_\infty\phi_6 && (49)
\end{aligned}$$

where X is exchanged for Y for the $z \to \infty$ limit where the laminar boundary conditions $U = 0$ and $V = -1$ can be applied. This gives $Y = \alpha^2 + \bar{\beta}^2 - iR(\bar{\beta} + \omega)$. The equations (44)–(49) have six independent solutions, ϕ_j^i, where i indicates the equation number and j is one of the six solutions. The solutions are given in the form $\phi_i^j(z \to \infty; \alpha, \omega, \beta; R) = c_i^j e^{K_j z}$ and can be substituted into the equations (44)–(49) to determine the constant coefficients c_i^j and K_j. The solutions

$$\begin{aligned}
K_{1,2} &= \frac{W_\infty}{2} \mp \left(\frac{W_\infty}{2}^2 + Y\right)^{\frac{1}{2}} && (50)\\
K_{3,4} &= K_{1,2} && (51)\\
K_{5,6} &= \mp\left(\alpha^2 + \bar{\beta}^2 - \frac{\alpha i}{R}\right)^{\frac{1}{2}} && (52)
\end{aligned}$$

are then found along with the c_i^j coefficients which can be found in appendix 4 of Lingwood (1995*b*). The values of ϕ_i^j and ϕ'^j_i at $z \to \infty$ are thus known and are used as the starting values for the shooting. The final solution vector then consists of the six independent solutions summed up for each equation, $\phi_i(z;, \alpha, \omega, \beta; R) = \sum_{j=1}^{6} C_j(\alpha, \omega, \beta; R)\phi_i^j(z; \alpha, \omega, \beta; R)$ where C_j is the weight for the specific solution. The summation of the different solutions should fulfills the boundary conditions, meaning at $z \to \infty$ all the perturbations must decay. To achieve this, K_j becomes such that $C_2 = C_4 = C_6 = 0$ due to their positive values. Already knowing this, it is only needed to solve for the solutions $j = 1, 3, 5$ and thus these are the only initial solutions considered in equations $i =$

$1-6$. These solutions are loaded for $z = 20$ assuming this distance is far enough from the wall to approximate $z \to \infty$.

To find the remaining weights C_1, C_3 and C_5, the boundary conditions at $z = 0$ are considered, also here the perturbation must decay. To obtain the values of C_1, C_3 and C_5 the equations must be integrated to this position, and then evaluated for proper weights. The integration is done by the RK4 method using equations (5)–(43). If there is no solution for C_1, C_3 and C_5 satisfying the boundary condition, the shooting parameter (α or ω) is updated according to the Newton–Raphson searching method and a new shooting takes place. The shooting is thus done from $z = 20$ to $z = 0$ also performing an orthonormalization if needed. Then an evaluation of the boundary conditions is done at $z = 0$ calculating a determinant described below.

To determine the weights C_1, C_3 and C_5, the determinant of $\mathbf{B}$ is evaluated to be zero within a certain tolerance level in the equation system $\mathbf{A} = \mathbf{Bx}$:

$$\begin{pmatrix} \phi_1 \\ \phi_3 \\ \phi_5 \end{pmatrix} = \begin{pmatrix} \phi_1^1 & \phi_1^3 & \phi_1^5 \\ \phi_3^1 & \phi_3^3 & \phi_3^5 \\ \phi_5^1 & \phi_5^3 & \phi_5^5 \end{pmatrix} \begin{pmatrix} C_1 \\ C_3 \\ C_5 \end{pmatrix} = \begin{pmatrix} 0 \\ 0 \\ 0 \end{pmatrix}. \tag{53}$$

When the determinant is zero, the variables α, β and ω satisfy the dispersion relation and are eigenvalues of the system at the considered R. At this stage the weights of C_1, C_3 and C_5 are found using the single value decomposition making it possible to reconstruct the solution. When the weights are obtained, the solution ϕ_1 can be constructed from ϕ_1^j and so forth until ϕ_6, where $j = 1, 3, 5$. This is done for all z positions where, if necessary, the solution is also reorthonormalized. This final step creates the eigenfunctions. From ϕ_1, ϕ_3 and ϕ_5 these transformed variables can be converted to the primitive variables $\hat{u}$,$\hat{v}$, $\hat{w}$ and $\hat{p}$.

3.2. *Spectral method by Chebyshev polynomials*

As an alternative method to analyse the linear stability, a spectral method using Chebyshev polynomials is applied. Here the equations (28)–(31) are set up as a large matrix and eigenvalues of this matrix are extracted. An advantage over the shooting method is that the perturbation equations are not transformed to a new system, and also for this method all eigenvalues are found at the same time instead of looking for one by one by using a qualified guess. A disadvantage is that only eigenvalues of ω are found.

The first step in this method is to define the Chebyshev polynomials in terms of trigonometric function as

$$T_n(y_j) = \cos(n \cos^{-1}(y_j)), \qquad n = 0, 1, \cdots, N \tag{54}$$

where N is number of collocation points and the Gauss–Lobatto points y_j are

$$y_j = \cos\left(\frac{j\pi}{N}\right), \qquad j = 0, 1, \cdots, N \tag{55}$$

therefore y_j satisfies a range of $-1 \leqq y_j \leqq 1$. The recurrence relations of the trigonometric function is given as

$$\begin{aligned} T_0(y_j) &= 1, && (56)\\ T_1(y_j) &= y_j, && (57)\\ T_{n+1}(y_j) &= 2yT_n(y_j) - T_{n-1}(y_j), && (58) \end{aligned}$$

which are the so-called Chebyshev polynomials of the first kind. Assuming that a function $f(y_j)$ is decomposed by Chebyshev expansions,

$$f(y_j) = \sum_{n=0}^{N} a_n T_n(y_j). \tag{59}$$

In addition, the derivatives of Chebyshev polynomials are defined as

$$\begin{aligned} T_0^{(k)}(y_j) &= 0, && (60)\\ T_1^{(k)}(y_j) &= T_0^{(k-1)}(y_j), && (61)\\ T_2^{(k)}(y_j) &= 4T_1^{(k-1)}(y_j), && (62)\\ T_n^{(k)}(y_j) &= 2nT_{n-1}^{(k-1)}(y_j) + \frac{n}{n-2}T_{n-1}^{(k)}(y_j), \quad n = 3, 4, \cdots, N, && (63) \end{aligned}$$

where k is the order of the derivative.

To introduce these Chebyshev expansions into an eigenvalue problems of the local linearized Navier–Stokes equations for the rotating-disk flow, the following procedures are applied. First, since the maximum wall-normal height is set to $z_{max} = 20$, a linear relation of the wall-normal height to y_j is given as

$$z_j = \frac{z_{max}}{2}(y_j + 1). \tag{64}$$

The Chebyshev polynomials and the derivatives for rotating-disk flow are given as

$$\begin{aligned} S_n(y_j) &= T_n(y_j), && (65)\\ S_n'(y_j) &= \frac{\mathrm{d}T_n(y_j)}{\mathrm{d}z} = T_n'(y_j)\frac{\mathrm{d}y}{\mathrm{d}z}, && (66)\\ S_n''(y_j) &= \frac{\mathrm{d}^2T_n(y_j)}{\mathrm{d}z^2} = T_n''(y_j)\left(\frac{\mathrm{d}y}{\mathrm{d}z}\right)^2 + T_n'\frac{\mathrm{d}y^2}{\mathrm{d}z^2}, && (67) \end{aligned}$$

where $'$ and $''$ of S_n mean the first and second derivatives in z, and the ones of T_n mean in y. Therefore eigenfunctions of the u, v, w, p components and the derivatives are expanded as

$$\begin{aligned} \hat{u}(y_j) = \sum_{n=0}^{N} a_n^{\hat{u}} S_n(y_j), \quad \hat{v}(y_j) = \sum_{n=0}^{N} a_n^{\hat{v}} S_n(y_j),\\ \hat{w}(y_j) = \sum_{n=0}^{N} a_n^{\hat{w}} S_n(y_j), \quad \hat{p}(y_j) = \sum_{n=0}^{N} a_n^{\hat{p}} S_n(y_j), \end{aligned} \tag{68}$$

$$\begin{aligned}\hat{u}'(y_j) &= \sum_{n=0}^{N} a_n^{\hat{u}} S_n'(y_j), \quad \hat{v}'(y_j) = \sum_{n=0}^{N} a_n^{\hat{v}} S_n'(y_j), \\ \hat{w}'(y_j) &= \sum_{n=0}^{N} a_n^{\hat{w}} S_n'(y_j), \quad \hat{p}'(y_j) = \sum_{n=0}^{N} a_n^{\hat{p}} S_n'(y_j),\end{aligned} \tag{69}$$

$$\hat{u}''(y_j) = \sum_{n=0}^{N} a_n^{\hat{u}} S_n''(y_j), \quad \hat{v}''(y_j) = \sum_{n=0}^{N} a_n^{\hat{v}} S_n''(y_j), \quad \hat{w}''(y_j) = \sum_{n=0}^{N} a_n^{\hat{w}} S_n''(y_j). \tag{70}$$

Now turning to the boundary conditions which are the same as in section 3.1, thus all perturbations should decay at $z \to \infty$. At the wall, velocity perturbations must be zero and from equation (28), it is found that the first derivative of $\hat{w}$ should also be zero. Therefore the boundary conditions at top and bottom of the domain are

$$\hat{u}(y_0) = \sum_{n=0}^{N} a_n^{\hat{u}} S_n(y_0) = 0, \quad \hat{v}(y_0) = \sum_{n=0}^{N} a_n^{\hat{v}} S_n(y_0) = 0, \tag{71}$$

$$\hat{w}(y_0) = \sum_{n=0}^{N} a_n^{\hat{w}} S_n(y_0) = 0, \quad \hat{p}(y_0) = \sum_{n=0}^{N} a_n^{\hat{p}} S_n(y_0) = 0, \tag{72}$$

$$\hat{u}(y_N) = \sum_{n=0}^{N} a_n^{\hat{u}} S_n(y_N) = 0, \quad \hat{v}(y_N) = \sum_{n=0}^{N} a_n^{\hat{v}} S_n(y_N) = 0, \tag{73}$$

$$\hat{w}(y_N) = \sum_{n=0}^{N} a_n^{\hat{w}} S_n(y_N) = 0, \quad \hat{w'}(y_N) = \sum_{n=0}^{N} a_n^{\hat{w}} S_n'(y_N) = 0. \tag{74}$$

Then the eigenvalue problem for ω is solved using equations (28)–(31) with the above boundary condition, given as

$$\boldsymbol{AV} = \boldsymbol{BVD}. \tag{75}$$

Equations (76)–(82) describe details of the matrix in equation (75). In equation (80), ϵ indicates a complex value carefully selected to perturb the matrix. In this study $\epsilon = -2000i$ is selected, where i is $\sqrt{-1}$. The columns in equation (81) shows each a mode of eigenfunctions. Eigenvalues are contained in equation (82) in diagonal direction.

We solve this eigenvalue problem in MATLAB with sets of conditions, R, α, β and mean velocity profiles for rotating-disk flow. Using obtained eigenfunctions in equation (81) and equation (68), we can produce eigenfunctions for u, v, w, p components.

$$\boldsymbol{A} = \begin{pmatrix}
S_n(y_0) & 0 & 0 & 0 & \cdots \\
0 & S_n(y_0) & 0 & 0 & \cdots \\
0 & 0 & S_n(y_0) & 0 & \cdots \\
0 & 0 & 0 & S_n(y_0) & \cdots \\
XX_0(y_1) & -2(1+V(y_1))/RS_0(y_1) & U'(y_1)S_0(y_1) & i\alpha S_0(y_1) & \cdots \\
2(1+V(y_1))/RS_0(y_1) & YY_0(y_1) & V'(y_1)S_0(y_1) & i\beta/RS_0(y_1) & \cdots \\
0 & 0 & ZZ_0(y_1) & S_0'(y_1) & \cdots \\
(i\alpha+1/R)S_0(y_1) & i\beta/RS_0(y_1) & S_0'(y_1) & 0 & \cdots \\
\vdots & \vdots & \vdots & \vdots & \\
XS_0(y_{N-1}) & -2(1+V(y_{N-1}))/RS_0(y_{N-1}) & U'(y_{N-1})S_0(y_{N-1}) & i\alpha S_0(y_{N-1}) & \cdots \\
2(1+V(y_{N-1}))/RS_0(y_{N-1}) & YY_0(y_{N-1}) & V'(y_{N-1})S_0(y_{N-1}) & i\beta/RS_0(y_{N-1}) & \cdots \\
0 & 0 & ZZ_0(y_{N-1}) & S_0'(y_{N-1}) & \cdots \\
(i\alpha+1/R)S_0(y_{N-1}) & i\beta/RS_0(y_{N-1}) & S_0'(y_{N-1}) & 0 & \cdots \\
S_n(y_0) & 0 & 0 & 0 & \cdots \\
0 & S_n(y_0) & 0 & 0 & \cdots \\
0 & 0 & S_n(y_0) & 0 & \cdots \\
0 & 0 & S_n'(y_0) & 0 & \cdots
\end{pmatrix} \tag{76}$$

$$XX_n(y_j) = (i\alpha U(y_j) + i\beta V(y_j)/R + \alpha^2/R + \beta^2/R^3 + U(y_j)/R)S_n(y_j) + W(y_j)/RS_n'(y_j) - 1/RS_n''(y_j) \tag{77}$$

$$YY_n(y_j) = (i\alpha U(y_j) + i\beta V(y_j)/R + \alpha^2/R + \beta^2/R^3 + U(y_j)/R)S_n(y_j) + W(y_j)/RS_n'(y_j) - 1/RS_n''(y_j) \tag{78}$$

$$ZZ_n(y_j) = (i\alpha U(y_j) + i\beta V(y_j)/R + \alpha^2/R + \beta^2/R^3 + W'(y_j)/R)S_n(y_j) + W(y_j)/RS_n'(y_j) - 1/RS_n''(y_j) \tag{79}$$

$$\boldsymbol{B} = \begin{pmatrix} \epsilon S_0(y_0) & 0 & 0 & 0 & \cdots \\ 0 & \epsilon S_0(y_0) & 0 & 0 & \cdots \\ 0 & 0 & \epsilon S_0(y_0) & 0 & \cdots \\ 0 & 0 & 0 & \epsilon S_0(y_0) & \cdots \\ iS_0(y_1) & 0 & 0 & 0 & \cdots \\ 0 & iS_0(y_1) & 0 & 0 & \cdots \\ 0 & 0 & iS_0(y_1) & 0 & \cdots \\ 0 & 0 & 0 & 0 & \cdots \\ \vdots & \vdots & \vdots & \vdots & \\ iS_0(y_{N-1}) & 0 & 0 & 0 & \cdots \\ 0 & iS_0(y_{N-1}) & 0 & 0 & \cdots \\ 0 & 0 & iS_0(y_{N-1}) & 0 & \cdots \\ 0 & 0 & 0 & 0 & \cdots \\ \epsilon S_0(y_N) & 0 & 0 & 0 & \cdots \\ 0 & \epsilon S_0(y_N) & 0 & 0 & \cdots \\ 0 & 0 & \epsilon S_0(y_N) & 0 & \cdots \\ 0 & 0 & \epsilon S_0'(y_N) & 0 & \cdots \end{pmatrix} \tag{80}$$

$$\boldsymbol{V} = \begin{pmatrix} a_{0,0}^{\hat{u}} & a_{0,1}^{\hat{u}} & \cdots & a_{0,4(N+1)-1}^{\hat{u}} \\ a_{0,0}^{\hat{v}} & a_{0,1}^{\hat{v}} & \cdots & a_{0,4(N+1)-1}^{\hat{v}} \\ a_{0,0}^{\hat{w}} & a_{0,1}^{\hat{w}} & \cdots & a_{0,4(N+1)-1}^{\hat{w}} \\ a_{0,0}^{\hat{p}} & a_{0,1}^{\hat{p}} & \cdots & a_{0,4(N+1)-1}^{\hat{p}} \\ a_{1,0}^{\hat{u}} & a_{1,1}^{\hat{u}} & \cdots & a_{1,4(N+1)-1}^{\hat{u}} \\ a_{1,0}^{\hat{v}} & a_{1,1}^{\hat{v}} & \cdots & a_{1,4(N+1)-1}^{\hat{v}} \\ a_{1,0}^{\hat{w}} & a_{1,1}^{\hat{w}} & \cdots & a_{1,4(N+1)-1}^{\hat{w}} \\ a_{1,0}^{\hat{p}} & a_{1,1}^{\hat{p}} & \cdots & a_{1,4(N+1)-1}^{\hat{p}} \\ \vdots & \vdots & & \vdots \\ a_{N,0}^{\hat{u}} & a_{N,1}^{\hat{u}} & \cdots & a_{N,4(N+1)-1}^{\hat{u}} \\ a_{N,0}^{\hat{v}} & a_{N,1}^{\hat{v}} & \cdots & a_{N,4(N+1)-1}^{\hat{v}} \\ a_{N,0}^{\hat{w}} & a_{N,1}^{\hat{w}} & \cdots & a_{N,4(N+1)-1}^{\hat{w}} \\ a_{N,0}^{\hat{p}} & a_{N,1}^{\hat{p}} & \cdots & a_{N,4(N+1)-1}^{\hat{p}} \end{pmatrix} \tag{81}$$

$$\boldsymbol{D} = \begin{pmatrix} \omega_0 & 0 & \dots & & 0 \\ 0 & \omega_1 & & & \vdots \\ & & \omega_2 & & \\ \vdots & & & \ddots & 0 \\ 0 & \dots & & 0 & \omega_{4(N+1)-1} \end{pmatrix} \tag{82}$$

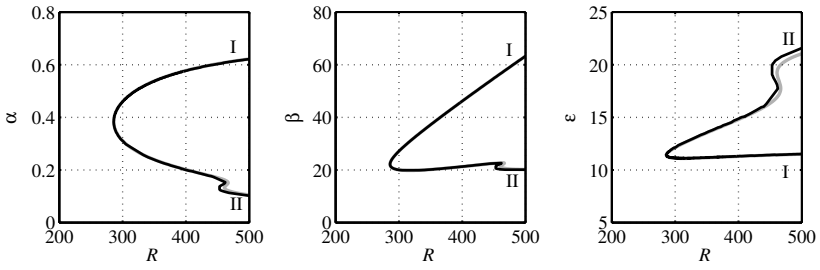

FIGURE 2. Neutral curve where the black line gives data from the shooting method and the grey line gives data from the Chebyshev method.

4. Results

4.1. *Neutral curves*

Figure 2 shows the neutral stability cuves given by both the Chebyshev and shooting methods. There is a small difference for the Type II region where the two codes converge to different values. This error was soley found to be due to the differences in the two methods. To estimate the difference, ω from the Chebyshev code was extracted on the neutral stability curve for the shooting method in the Type II area. While keeping $\alpha_i = \beta_i = 0$, ω had an absolute value of the order 10^{-6}.

4.2. *Eigenfunctions*

From local theory, the eigenfunctions of each velocity component were calculated for $R = 375$ and $\beta = 32$ of the Type-I mode ($\omega = 0$ and $\alpha = 0.44 - i0.024$) and were compared with experimental and DNS data. This data is presented in Appelquist *et al.* (2016).

5. Summary

The similarity solution for the rotating-disk boundary layer was calculated and a local linear stability analysis was performed for the rotating-disk boundary layer flow. Two methods, the shooting method and the Chebyshev polynomial method, were compared and both methods showed similar results for the neutral curves and eigenfunctions. There were slight differences in the viscous part of the neutral curves (Type-II), which was concluded to originate from the numerics used. An eigenfunction example also showed good agreement between the two methods and also with DNS and experimental data.

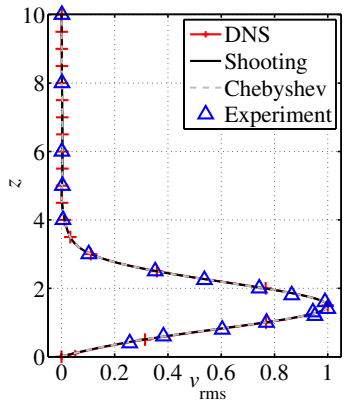

FIGURE 3. Eigenfunction of v_{rms} at $R = 375$ for $\beta = 32$ normalized by the maximum value. The local theory data have a fixed $\omega = 0$ and $\alpha = 0.44 - i0.024$. Experimental results ($\triangle$) of azimuthal unsteady disturbance amplitudes measured by hot-wire anemometry. All data are normalized by maximum amplitude of the azimuthal velocity component.

This is the second edition of the same paper appearing in Appelquist (2014). A figure of the Chebyshev polynomials has been taken away, there has been a correction to a typographical error in equation (79), and the result section has been modified. This is mainly due to a mistake that appears in one of the transformed variables for Mack (1985) which was the basis of an error analysis. Also the introduction is modified appropriately.

This work is supported by the Swedish Research Council through the ASTRID project and the Linné FLOW Centre. It was initated thanks to the NORDITA program on stability and transition in Stockholm, May 2013.
Many thanks to both Dr. Antonio Segalini for help writing the linear stability code using Chebyshev polynomials, and to Prof. R. J. Lingwood for input on the shooting method.

APPENDIX A

Solving the laminar von Kármán equations using the shooting method

In solving equations (8)–(11), the three first equations can be solved separately using five boundary conditions since there are five unknown variables, U, V, W, U' and V'. The values for W', U'' and V'' are then known from the equations. The boundary conditions used are: no slip at the wall, $U(0) = 0$ and $V(0) = 0$; $W(0) = 0$ due to the impermeability of the disk; and a far field boundary condition implying no viscous effects far from the wall giving $U(z \to \infty) = 0$ and $V(z \to \infty) = -1$. Including the last equation, (11), a sixth boundary condition for the pressure was used, $P(0) = 0$. This is then a reference level for the pressure profile. The system of equations can be transformed into a system of first order equations by letting $g_1 = U'$ and $g_2 = V'$. In equation (11), equation (8) is used for W' and W'' since also $W'' = -2U'$. The system of equations then becomes

$$
\begin{aligned}
g_1 &= U' && \text{(A-1)}\\
g_2 &= V' && \text{(A-2)}\\
W' &= -2U && \text{(A-3)}\\
g_1' &= U^2 - (V+1)^2 + g_1 W && \text{(A-4)}\\
g_2' &= 2U(V+1) + g_2 W && \text{(A-5)}\\
P' &= 2WU - 2g_1 && \text{(A-6)}
\end{aligned}
$$

For g_1 and g_2 there are no boundary conditions. Applying RK4 together with Newton–Raphson shooting, the boundary conditions at $z \to \infty$ are initially disregarded and g_1 and g_2 are set to initial guesses

$$g_1(0) = s_1 \quad \text{and} \quad g_2(0) = s_2. \tag{A-7}$$

These guesses, also called the shooting parameters, are evaluated after an RK4 integration such that the top boundary conditions $U(z_{max}) = 0$ and $V(z_{max}) = -1$ are satisfied, where $z_{max} = 20$ is considered to be sufficient.

Starting guesses of $s_1 = 0.52$ and $s_2 = -0.61$ were chosen (the equations turned out to be very sensitive to these first choices) and when the set of equations had been integrated to z_{max}, the residual functions $Z_1 =$

$U(z_{max}, s_1, s_2) - U(z_{max})$ and $Z_2 = V(z_{max}, s_1, s_2) - V(z_{max})$ could be evaluated. For perfect shooting parameters, these should correspond to zero at z_{max}. The shooting parameters are updated in every step to improve the residual functions, i.e. making them smaller,

$$\bar{s}^{n+1} = \bar{s}^n + \bar{h}^n \tag{A-8}$$

where $\bar{h}^n = J^{-1}\bar{Z}$ and $J(\bar{s})$ is the Jacobian containing the change in the solution U and V with respect to the shooting parameters, which can be found by using the equations for U'' and V'' from (A-4) and (A-5) (g_1' and g_2'). We are thus looking for $U_{S1} = \partial U(z_{max})/\partial s_1$, $U_{S2} = \partial U(z_{max})/\partial s_2$, $V_{S1} = \partial V(z_{max})/\partial s_1$ and $V_{S2} = \partial V(z_{max})/\partial s_2$ to go in the Jacobian. These can be obtained by differentiating equations (A-4) and (A-5) one more time with respect to s_1 and s_2 obtaining 4 equations, and then integrate these in z. The below equations are used for this;

$$\begin{aligned}
DU_{S1} &= U'_{S1} && \text{(A-9)}\\
DU_{S2} &= U'_{S2} && \text{(A-10)}\\
DDU_{S1} &= 2U \cdot U_{S1} + W \cdot DU_{S1} + g_1 \cdot W_{S1} - 2V \cdot V_{S1} - 2V_{S1} && \text{(A-11)}\\
DDU_{S2} &= 2U \cdot U_{S2} + W \cdot DU_{S2} + g_1 \cdot W_{S2} - 2V \cdot V_{S2} - 2V_{S2} && \text{(A-12)}\\
DV_{S1} &= V'_{S1} && \text{(A-13)}\\
DV_{S2} &= V'_{S2} && \text{(A-14)}\\
DDV_{S1} &= W \cdot DV_{S1} + g_2 \cdot W_{S1} + 2U \cdot V_{S1} + 2VU_{S1} + 2U_{S1} && \text{(A-15)}\\
DDV_{S2} &= W \cdot DV_{S2} + g_2 \cdot W_{S2} + 2U \cdot V_{S2} + 2VU_{S2} + 2U_{S2} && \text{(A-16)}\\
DW_{S1} &= -2U_{S1} && \text{(A-17)}\\
DW_{S2} &= -2U_{S2} && \text{(A-18)}
\end{aligned}$$

Equations (A-11)–(A-12) and (A-15)–(A-16) are the four new equations integrated with respect to $\bar{s}$ where D now also signals differentiation with respect to z for the solution terms, e.g. $DDU_{s1} = \partial U''/\partial s_1$. For the above 10 equations, 10 additional boundary conditions are needed. These are at $z = 0$; $\partial U/\partial s_1 = 0$, $\partial U'/\partial s_1 = 1$, $\partial U/\partial s_2 = 0$, $\partial U'/\partial s_2 = 0$, $\partial V/\partial s_1 = 0$, $\partial V'/\partial s_1 = 0$, $\partial V/\partial s_2 = 0$, $\partial V'/\partial s_2 = 1$, $\partial W/\partial s_1 = 0$ and $\partial W/\partial s_2 = 0$. Solving the (A-1)–(A-6) and (A-9)–(A-18) as a system, the result plotted in figure 1 for U, V, W and P is found. When solving the equations, 10 iterations gave a residual less than 10^{-3} for both Z_1 and Z_2, and 53 iterations gave a residual in the order of 10^{-16}. The equations also turned out to be sensitive to changing the height of the domain, however, for $z \leq 20$ the method is robust. At this z level, $\mathrm{d}U/\mathrm{d}z$ and $\mathrm{d}V/\mathrm{d}z$ are of the order of 10^{-8}.

Bibliography

Appelquist, E. 2014 Direct numerical simulations of the rotating-disk boundary-layer flow. Licentiate thesis, Royal Institute of Technology, KTH Mechanics, ISBN: 978-91-7595-202-4.

Appelquist, E., Imayama, S., Alfredsson, P. H., Schlatter, P. & Lingwood, R. J. 2016 Linear disturbances in the rotating-disk flow: a comparison between results from simulations, experiments and theory. *Euro. J. Mech. B/Fluids* **55**, 170–181.

Arco, E. D., Serre, E. & Bontoux, P. 2005 *Stability, Transition and Turbulence in Rotating Cavities*. WIT Press.

Balakumar, P. & Malik, M. R. 1990 Traveling disturbances in rotating-disk flow. *Theor. Comp. Fluid. Dyn.* **2**, 125–137.

Faller, A. J. 1991 Instability and transition of disturbed flow over a rotating disk. *J. Fluid Mech.* **230**, 245.

Hussain, Z., Garrett, S. J. & Stephen, S. O. 2011 The instability of the boundary layer over a disk rotating in an enforced axial flow. *Phys. Fluids* **23**, 114108.

Hwang, Y. K. & Lee, Y. Y. 2000 Theoretical flow instability of the Kármán boundary layer. *KSME Int. J.* **14**, 358 – 368.

Imayama, S., Alfredsson, P. H. & Lingwood, R. J. 2013 An experimental study of edge effects on rotating-disk transition. *J. Fluid Mech.* **716**, 638–657.

von Kármán, T. 1921 Über laminare und turbulent Reibung. *Z. Angew. Math. Mech.* **1**, 233–252.

Kobayashi, R., Kohama, Y. & Takamadate, C. 1980 Spiral vortices in boundary layer transition regime on a rotating disk. *Acta Mech.* **35**, 71–82.

Lingwood, R. J. 1995*a* Absolute instability of the boundary layer on a rotating disk. *J. Fluid Mech.* **299**, 17–33.

Lingwood, R. J. 1995*b* Stability and Transition of the Boundary Layer on a Rotating Disk. Phd thesis, Cambridge Unniversity.

Lingwood, R. J. 1997 Absolute instability of the Ekman layer and related rotating flows. *J. Fluid Mech.* **331**, 405–428.

Mack, L. 1985 The wave pattern produced by a point source on a rotating disk. *AIAA Paper* (85–0490).

Malik, M. R. 1986 The neutral curve for stationary disturbances in rotating-disk flow. *J. Fluid Mech.* **164**, 275–287.

Malik, M. R., Wilkinson, S. P. & Orszag, S. A. 1981 Instability and transition in rotating disk flow. *AIAA J.* **19**, 1131–1138.

Pier, B. 2003 Finite-amplitude crossflow vortices, secondary instability and transition in the rotating-disk boundary layer. *J. Fluid Mech.* **487**, 315–343.